5.3 FINE PARTICULATE MATTER MODELING IN CENTRAL CALIFORNIA
# PART I: APPLICATION OF THE WEATHER RESEARCH AND FORECASTING MODEL

Raphael Rogers[1], Aijun Deng[1]*, David Stauffer[1], Yiqin Jia[2], Su-Tzai Soong[2], Saffet Tanrikulu[2], Scott Beaver[2], and Cuong Tran[2]

[1] Pennsylvania State University, University Park, PA
[2] Bay Area Air Quality Management District, San Francisco, CA

## 1. INTRODUCTION

Photochemical air quality models such as the Community Multiscale Air Quality (CMAQ) Model and the ENVIRON International Corporation's Comprehensive Air Quality Model with Extensions (CAMx) are widely used to simulate particulate matter (PM), air toxics, and ozone concentrations. Accurate meteorological information as input to air chemistry models is critically important for air quality modeling (e.g., Tanrikulu et al. 2000, Deng et al. 2004, Otte 2008a, b).

The Bay Area Air Quality Management District (BAAQMD) has been using the CMAQ and CAMx models to simulate air pollution concentrations in the San Francisco Bay Area, with meteorological inputs provided using the Penn State-National Center for Atmospheric Research (NCAR) Mesoscale Model Version 5 (MM5) (Grell et. al, 1994). Development of the MM5 system has been discontinued. Therefore, the BAAQMD is interested in transitioning to the Weather Research and Forecasting (WRF) model (Skamarock et al. 2008), a newly developed mesoscale modeling system that is widely supported by the research and operational communities. Similar to MM5, the WRF model encompasses many model physics schemes and has four-dimensional data assimilation (FDDA) capabilities that were recently implemented by Penn State (Deng et al. 2009). The BAAQMD's goal is to transition to the WRF model when it can perform as well as the MM5.

The purpose of this study is to determine the optimal WRF model configuration for air quality modeling over the San Francisco Bay Area region. Both summer and winter cases are modeled. The Bay Area is part of the larger central California modeling domain that also covers the Sacramento and San Joaquin Valleys to the east. This domain has nested 36-, 12-, and 4-km horizontal grids (Figure 1). Evaluations of the WRF model performance using different model physics and FDDA strategies are conducted. The WRF outputs for the innermost 4-km domain are used to drive air quality simulations that are evaluated in the second part of this two-part study (Beaver et al., 2011).

* *Corresponding author address*: Aijun Deng, Department of Meteorology, 503 Walker Building, Pennsylvania State University, University Park, PA 16802; e-mail: deng@meteo.psu.edu

Section 2 gives a description of the meteorological model used for this study. Section 3 provides descriptions for both the winter case and the summer case, and the model setup and a description of the model experiments are given in section 4. Results of the WRF model evaluation comparing the model physics and the FDDA strategies are presented in section 5. Conclusions and future work are presented in section 6

## 2. METEOROLOGICAL MODEL DESCRIPTION

The meteorological model used in this study is the advanced research dynamics solver of the WRF model (WRF-ARW, Skamarock et al. 2008). The WRF model is a new state-of-the-science mesoscale community-supported NWP model that is under continuous development. Currently there are two versions of the WRF model available for the research and forecast communities: the NCAR WRF-ARW and the National Centers for Environmental Prediction (NCEP) Non-hydrostatic Mesoscale Model (WRF-NMM).

Similar to MM5, the WRF-ARW is also a nonhydrostatic, fully compressible three dimensional primitive equation model with a terrain-following vertical coordinate, denoted by $\eta$ that is defined by hydrostatic pressure of the dry atmosphere. For temporal discretization, the WRF-ARW solver uses a third-order Runge-Kutta (Skamarock et al. 2008) time integration scheme, while the high-frequency acoustic modes are integrated over smaller time steps to maintain numerical stability. For spatial discretization, the WRF-ARW solver uses Arakawa-C horizontal grid staggering, in which normal velocities are staggered one-half grid length from the thermodynamic variables. In the vertical direction, variables are defined with wind and mass field on half $\eta$ layers and the vertical velocity and TKE at the full layers.

There are a number of formulations for turbulent mixing and filtering available in the WRF-ARW solver. Some of them are used for numerical reasons, and other filters are meant to represent physical subgrid turbulent processes. Unlike MM5, the WRF-ARW allows sub-grid scale turbulence to be parameterized as it is treated in cloud-scale models – including horizontal mixing.

The WRF-ARW has a variety of physics options for microphysics, cumulus parameterization, atmospheric radiation, and planetary boundary layer (PBL) / turbulence physics that can interact with the model's dynamics and thermodynamics. The explicit microphysics predicts grid-resolved water vapor, cloud and precipitation processes, while the cumulus parameterization accounts for subgrid-scale vapor, cloud and precipitation processes. The radiation schemes provide atmospheric heating due to radiative flux divergence and surface downward longwave and shortwave radiation for the ground heat budget. Unlike MM5, the WRF-ARW surface layer physics is treated outside of the PBL scheme although specific surface layer options can be tied to particular boundary-layer options.

WRF also has several land-surface models (LSMs) that use atmospheric information from the surface layer scheme, radiative forcing from the radiation scheme, and precipitation forcing from the microphysics and convective schemes, together with internal information on the land's state variables and land-surface properties, to predict heat and moisture fluxes to the atmosphere. These fluxes provide a lower boundary condition for the vertical transport represented in the PBL schemes.

*a. Relevant Model Physics*

The microphysics option used in the model simulations is the WRF Single-Moment 3-class (WSM3) simple ice scheme, which does not allow mixed phases of hydrometeors. Two atmospheric radiation schemes are compared to determine the best radiation scheme for the simulations: 1) Rapid Radiative Transfer Model (RRTM, Mlawer et al. 1997), and 2) the Rapid Radiative Transfer Method for GCMs (RRTMG, Mlawer et al. 1997, Iacono et al. 2008). As in MM5, the RRTM scheme is used for longwave radiation in combination with the Dudhia scheme (Dudhia 1989) for shortwave radiation. The RRTMG scheme that was originally designed for global circulation models (GCMs) and recently implemented into WRF-ARW is also used for both longwave and shortwave radiation in our study.

To determine the best LSM for the simulations, the 5-layer thermal diffusion scheme is used and compared with three LSMs: 1) Noah LSM (Chen and Dudhia 2001), 2) Rapid Update Cycle (RUC, Smirnova et al., 1997, 2000) LSM, and 3) Pleim-Xiu (PX) LSM (Pleim and Xiu, 1995; Xiu and Pleim, 2001). The Kain-Fritsch scheme (Kain and Fritsch 1990, Kain 2004) is used for the cumulus parameterization on the 36- and 12-km grids. The PBL physics used in this study is the TKE-predicting Mellor-Yamada Level 2.5 turbulent closure scheme (Janjic 1996, 2002), except when the PX physics is used. This requires the PBL physics ACM2 (the asymmetrical convective model version 2) which is designed for the PX physics suite.

*b. Four-Dimensional Data Assimilation*

Four-dimensional data assimilation (FDDA) used in this research was originally developed at Penn State (Stauffer and Seaman 1990, 1994) and was recently enhanced and implemented into WRF-ARW (Deng et al. 2009). In nudging FDDA, the model state is relaxed continuously toward the observed state at each time step by adding an artificial tendency term, which is based on the difference between the two states, to the prognostic equations. Data assimilation can be accomplished by nudging the model solutions toward gridded analyses based on observations (analysis nudging), or directly toward the individual observations (observation nudging), within a multiscale grid-nesting assimilation framework typically using a combination of these two approaches.

In analysis nudging, the model fields are nudged at every grid point toward an analysis of the observations on the model grid in a manner such that the nudging term is proportional to the difference between the model and the analysis at each grid point. In observation nudging, the model solution is nudged toward the observations within the given radius of influence near the observation locations, and within the given time window surrounding the observations.

The nudging term is smaller in magnitude than any of the other terms in the equations so that the it does not control the tendency. If the nudging is too strong, the model may lose important mesoscale features created by the model. But, if it is too weak, the observations will have a minimal effect on the evolution of the model state, allowing phase and amplitude errors to grow. For this reason, the value of the nudging factor should be carefully defined.

In WRF-ARW, the following equation represents a nudging term for potential temperature or any general predictive variable in WRF, coupled with the dry hydrostatic pressure $\mu$, where

$$\Theta = \mu \cdot \theta \tag{1}$$

and the prognostic equation including the nudging terms becomes

$$\begin{aligned} \frac{\partial \Theta}{\partial t} &= \cdots + \mu \frac{\partial \theta}{\partial t} + \theta \frac{\partial \mu}{\partial t} \\ &= \cdots + \mu \cdot G_\theta \cdot W \cdot (\theta_{ob} - \theta) + \theta \cdot G_\mu \cdot W \cdot (\mu_{ob} - \mu) \end{aligned} \tag{2}$$

where the four-dimensional weighting function is given by $W = w_{xy} \cdot w_\eta \cdot w_t$, the nudging coefficient is G, and 1/G is the e-folding time, which is a representative time scale for the artificial nudging term. This time scale should be longer than the time scale of the slowest physical process in the model. Currently in WRF-ARW, both analysis nudging and observation nudging can be applied to u (west-east wind component), v (south-north wind component), θ (potential temperature), and $q_v$ (water vapor mixing ratio).

Further development of obs nudging in WRF-ARW has brought more flexibility in how surface wind observations are spread in the vertical. As illustrated in Fig. 2, WRF users have freedom to choose different vertical weighting functions for the surface observations. In contrast, the MM5 obs nudging capability has surface winds spread through the lowest three model layers with linearly-decreasing weights for all PBL regimes (column 5 in Fig. 2), as the default. WRF allows the surface obs to be spread through the entire PBL with full strength then linearly decreases to zero 50 m above the PBL top for the unstable PBL regime (regime 4, column 3 in Fig. 2). For the stable PBL regimes (regimes 1 and 2), as the default, WRF allows the surface obs to be spread upward to 50 m with full strength and then linearly decreases to zero for the next 50m. In this study the default surface data weighting functions are used.

## 3. CASE DESCRIPTION

Two air pollution cases are chosen for this modeling study, a winter PM case and a summer ozone case. The winter PM case period is from 12 UTC on December 16, 2000 to 12 UTC on December 21, 2000. The summer ozone case period is from 12 UTC on July 29, 2000 to 12 UTC on August 3, 2000.

### *a. Winter PM case*

At the beginning of the winter PM case period a weak surface trough is just offshore of the California coast and a high is centered over Nevada (Fig. 3). There is surface northwesterly flow in the San Francisco Bay Area and the Central Valley region; and there is a large ridge at 500 hPa at this time that is also leading to northwesterly winds at 500 hPa over the entire region. Over the course of the next two days a cold front moves through the region and a high moves onshore from the Pacific Ocean. At 500 hPa a trough quickly moves through and another ridge moves onshore leading to westerly flow over the Bay Area. The surface winds over the region become easterly. As the surface high continues to move eastward over the next day (19 Dec. 2000) the winds become northerly in the valley and southerly over the Bay Area. By the end of the period high pressure dominates the western United States and the winds over the Bay Area and Central Valley remain northerly. The ridge at 500 hPa remains over the region for the rest of the study period and westerly flow dominates over the region.

### *b. Summer ozone case*

This summer ozone case is similar to the one studied and described by Bao et al. 2008. A ridge of high pressure at 500 hPa is over the San Francisco Bay Area and the Central Valley region and the ridge strengthens over the first two days. The ridge allowed for very high temperatures with the temperature over Oakland reaching 27$^{o}$C at 850 hPa, and at the surface the ridge caused the low-level winds in the Central Valley region of California to become weak. These weak winds allow for high pollution episodes. By the end of the period a trough moves onshore, which allows the winds over the Central Valley to become stronger and cools the temperatures in the region. During the entire period the 500 hPa winds over the San Francisco Bay Area and the Central Valley are southerly and southeasterly (Fig. 3 from Bao et al. 2008).

## 4. EXPERIMENTAL DESIGN

### *a. WRF Modeling Configuration*

For this study the model configuration is comprised of three domains: 36-km, 12-km, and 4-km as shown in Fig. 1. The 36-km domain, with a mesh of 91x95 grid points, contains the entire western United States, parts of Mexico and Canada, and a large area of the eastern Pacific Ocean. The 12-km domain, with a mesh of 157x151 grid points, contains the entire state of California, the states of Oregon and Nevada, parts of Idaho, Utah, Wyoming, Arizona, and Montana, parts of Mexico and the Pacific Ocean. The 4-km domain, with a mesh of 190x190 grid points, contains the entire central California air quality modeling domain. It consists of the San Francisco Bay Area and the Central Valley region that contains both the Sacramento Valley and the San Joaquin Valley. Fifty (50) vertical $\eta$ layers are used in all numerical experiments for all grids. The lowest half layer is located at ~12 m above ground level (AGL). The thickness of the layers increases gradually with height, with 26 layers below 850 hPa (~1550 m AGL). The top of the model is set at 100 hPa. One-way nesting is used for all experiments so that information from the coarse domains translates to the fine domains but no information from the fine domains translate to the coarse domains. The model simulations use the 40-km Eta analyses for the initial conditions/lateral boundary conditions. The initial condition fields are further enhanced by rawinsonde and surface data through WRF objective analysis process, OBSGRID (Deng et al. 2009), using a modified Cressman analysis (Benjamin and Seaman 1985). The lateral boundary conditions and three-dimensional (3D) analyses used for analysis FDDA are also enhanced by the objective analysis process and are defined at 6-h intervals, and surface analysis fields used for surface analysis FDDA are generated by OBSGRID at 3-h intervals.

Quality-checked (QC) WMO 12-hourly sondes and hourly surface observations are also used to create the QC-ed observations (Fig. 4a) needed for both obs nudging and model verification. In addition to the WMO observations, there are special wind profiler observations from 19 stations (Fig. 4b), and special surface wind observations from about 90 stations located in the valleys. All of these data are QC-ed by OBSGRID (using a high-resolution version of the WPS/UNGRIB software).

### *b. Model Experiments*

To find the optimal WRF model configuration for the region, various WRF experiments, with varying model physics and FDDA options, are conducted. The WRF solutions are verified against the WMO surface and upper air observations. The investigation started with comparing the use of two commonly used atmospheric radiation schemes, RRTM/Dudhia and RRTMG. As indicated later in the results section, the RRTM scheme was decided to be used for all the rest numerical experiments. The next step is to determine an optimal LSM for the region since CMAQ model used at BAAQMD is customized to use the land surface fields as input to the air chemistry model. It was found for the winter PM case period that the PX physics has a clear advantage (see details later in the results section). For the summer the ozone case period, the results based on different LSM are quite mixed. Based on the BAAQMD's previous experience with PX physics, a decision was made to use the PX for all the rest of the experiments involving FDDA. As indicated in Section 2, for both the winter PM and the summer ozone cases, all FDDA experiments use WSM3 simple ice microphysics, K-F cumulus parameterization on the 36- and 12-km grids, and ACM2 PBL scheme as part of the PX physics suite.

*i. Winter PM case FDDA experimental design*

Using the best model physics found as the result of sensitivity study for atmospheric radiation and land surface processes as the baseline model configuration, a set of six model simulations is performed for the winter PM case period (Table 1): 1) NOFDDA, no data assimilation of any form is used; 2) GFDDA, 3D (excluding surface) analysis nudging is used on the 36-km and 12-km domains; 3) OFDDA, only obs nudging is used on all three domains, assimilating WMO and special wind profiler data; 4) MFDDA, multiscale FDDA combining 3-D analysis nudging (on the 36- and 12-km domains) and obs nudging (on all domains) in a multiscale FDDA framework is used as shown in Table 2; 5) MFDDA2, same as MFDDA experiment except surface analysis nudging is used, including the soil temperature nudging (Pleim and Gilliam 2009) that is automatically activated when the surface analysis nudging is used with PX physics; and 6), MFDDA3, same as MFDDA2 except soil temperature nudging are turned off. The purpose of the Expt. MFDDA3 is to evaluate the effects of using soil temperature nudging.

The parameters used in the FDDA experiments are shown in Table 2. Nudging of the wind field is applied though all model layers, but nudging for the mass field is only allowed above the model-simulated PBL. A time window of two hours is used in obs nudging for upper air observations, with a reduced window of one hour at the surface. A reduced radius of influence (i.e. by multiplying a factor of 0.67 to the specified value in Table 2) for surface data is also used. Note that as indicated in Table 2, in the multiscale FDDA framework, the analysis nudging is applied on the 12-km grid with reduced strength (from 0.0003 to 0.0001).

*ii. Summer ozone case FDDA experimental design*

For the summer ozone case period, a set of three model simulations is conducted (Table 3), 1) NOFDDA, no data assimilation of any form is used; 2) MFDDA4, similar to the MFDDA2 experiment from the winter case, and only the WMO observations are assimilated; and 3) MFDDA5, same as MFDDA4, except the simulation also assimilates the BAAQMD special surface observations in addition to the WMO observations. Expt. MFDDA5 is designed to show the added value of assimilating the special surface observations of the BAAQMD meteorological network.

The FDDA parameters are the same for the winter case shown in Table 2 except there is no observational nudging on the 36-km domain. The observational-nudging is turned off on this domain to gauge how the 4-km domain is affected when there is no observational nudging information being passed from the 36-km domain to the 12-km domain which in turn passes information to the 4-km domain. As expected the difference in the 4-km WRF solutions between the experiment with and without 36-km obs nudging is minimal and can be neglected.

Compared to the default WRF model used in the winter PM case, the WRF model used for the summer ozone case period includes two of the recent Penn State modifications in WRF obs nudging capability. The first modification allows WRF obs nudging to use an MM5 method (Stauffer and Seaman 2004) to define the horizontal radius of influence especially important in complex terrain. The WRF default method can produce adverse effects of the observations' influence over complex terrain. Comparison of the WRF solutions using the two different methods indicated that the MM5 method has a slight advantage. The second modification allows the lowest sounding level to be treated like the regular surface observations in terms of how surface obs are spread horizontally.

## 5. METEOROLOGICAL RESULTS

Evaluation of simulated meteorological features is accomplished by both objective and subjective methods. Objective evaluation is first performed by comparing the statistical scores (i.e., mean absolute error, MAE) of the model-simulated wind speed, wind direction, temperature and water vapor mixing ratio. The subjective analysis includes comparison of the model-simulated mesoscale structures to the observed features (e.g., mesoscale eddies and down-slope and up-slope flows).

*a. Winter PM Case*

The investigation begins with comparing the WRF solutions between using the RRTM and the RRTMG radiation schemes. It is found that both radiative schemes produce similar results for all verification fields (i.e. wind speed, wind direction, temperature and water vapor mixing ratio), with a slight degradation shown in some fields in the RRTMG experiment. As an example, Fig. 5 shows the MAE of the WRF-simulated surface-layer temperature between the RRTM radiation scheme and the RRTMG radiation scheme. The red bars are the results for the 36-km domain, the green bars are for the 12-km domain, and the blue bars are for the 4-km domain. It is shown that WRF-simulated surface-layer temperature MAE is nearly identical for both 36- and 4-km grids, and there is a slight degradation when RRTMG is used for the 12-km grid. Considering the fact that most air-pollution cases are under weakly-forced fair weather conditions, WRF with varying atmospheric radiation schemes will less likely produce dramatically different solutions. Therefore, all of the numerical experiments use the RRTM/Dudhia radiation scheme.

To determine an optimal LSM to use, the MAE of the WRF-simulated fields is compared among the 5-layer thermal diffusion scheme, the Noah LSM, the RUC LSM, and the Pleim-Xiu (PX) LSM. Figure 6 shows the MAE of the WRF-simulated surface-layer relative humidity, temperature, wind direction, and wind speed (Figs. 6a, 6b, 6c, and 6d, respectively). Comparing the PX results with the results of the Noah and the RUC, we find quite a positive impact when using the PX physics. The PX physics generally produce better surface statistics than the 5-layer thermal diffusion scheme and the other two LSM schemes (only degrading the 4-km relative humidity and the 36-km wind direction). For upper air (not shown), the PX (as well as the Noah and the RUC) shows improvement from the 5-layer thermal diffusion scheme for relative humidity and wind direction. Similar to the Noah and the RUC, the PX also shows some degradation compared to the 5-layer thermal diffusion scheme for temperature and wind speed, but the degradation is smaller than that in the Noah and the RUC. Based on these findings, the Pleim-Xiu LSM is chosen as the LSM as part of the best model configuration.

Using the RRTM radiation scheme and the PX physics suite, various FDDA experiments are designed using the multiscale strategy. The MAE of the WRF-simulated surface fields for the set of FDDA simulations is shown in Fig. 7. The figures were made with the intent of having the worse model simulation on the far left and as we go to the right the model simulations show continual improvement with the best model simulation on the far right; this pattern will be called the "improvement trend". We don't necessarily see this trend for the relative humidity and temperature (Figs. 7a and 7b, respectively). The reason for this is because there is no nudging of the mass fields within the model-simulated PBL including the surface layer. However, the use of FDDA still shows some improvement over the No-FDDA simulation. The improvement trend is very evident for both the wind direction and the wind speed (Figs. 7c and 7d, respectively). Nudging is applied for the wind fields for all layers giving a large improvement in the model simulations that use FDDA, and especially those that use surface analysis nudging (MFDDA2 and MFDDA3). Both the MFDDA2 and MFDDA3 simulations give the best results; however turning off nudging of the soil temperature does not show much of a difference over keeping the soil moisture nudging on; therefore, the MFDDA2 is considered the optimal FDDA configuration for the surface.

Similar to the surface-layer results, Figure 8 shows the MAE for the four fields in the upper-air for the FDDA simulations. The improvement trend is very evident for all four fields because nudging is turned on for both the mass (above the PBL) and wind fields for the upper-air. The three MFDDA simulations show large improvement over the other three simulations with the MFDDA2 simulation giving the best results. Therefore, having both 3D and surface analysis nudging in combination with observational nudging gives the best model simulation for the winter case.

Figure 9 shows plots of the model-simulated surface winds, overlaid with WMO observations, on the 4-km domain at 00 UTC on December 17, 2000 (i.e., 4PM local time, 12 h into the simulation). Fig. 9a is a plot for a model simulation without FDDA and Fig. 9b is with FDDA. Even without FDDA the model does a reasonable job of capturing the mesoscale features. The model shows typical daytime northerly divergent flow along the San Joaquin Valley with upslope flow along the Coastal Ranges and the Sierra Nevada Mountains. There is also southerly flow in the Sacramento Valley but the flow is not as divergent as in the San Joaquin Valley. There is mostly northwesterly flow along the California coast and over the San Francisco Bay Area. The model has better agreement with the observations when FDDA is used. The model-simulated winds agree better with the observations over the Sacramento Valley and also the San Joaquin Valley. With the use of FDDA the model develops the westerly flow that is observed in the San Joaquin Valley at this time.

*b. Summer Ozone Case*

Similar sensitivity experiments using varying physics are conducted for the summer case, except for the atmospheric radiation physics. The synoptic conditions for the summer ozone are similar to the conditions for the winter case; there is a ridge of high pressure over the San Francisco Bay Area and the Central Valley region of California, and it brings dry conditions and very little moisture and precipitation to these areas. Therefore, the same RRTM scheme that is used for the winter PM case is chosen for the model simulations for the summer case as well.

The comparison among the Noah, RUC and PX LSMs indicates that not one particular LSM outperforms the others for all four fields on all the domains (not shown). Since the PX scheme is being developed at the U.S. EPA and is well-tested for air quality applications, the PX LSM is again chosen for the summer case.

Using the RRTM scheme as the atmospheric radiation physics and PX physics suite as the baseline simulation, two FDDA experiments are conducted and compared with the baseline. Figure 10 shows the MAE of the

WRF-simulated surface layer relative humidity, temperature, wind direction and wind speed, for all three experiments. The improvement trends for these simulations are similar to those for the winter case. There are some small improvements for the relative humidity and temperature fields (Figs. 10a and 10b, respectively) despite the fact that the mass fields are not directly assimilated within the PBL (Table 2). There are larger improvements for the wind direction and wind speed fields (Figs. 10c and 10d, respectively) due to assimilation of the wind fields. Since in addition to the WMO observations MFDDA5 also includes the 94 special surface wind observations, comparing MFDDA5 and MFDDA4 demonstrates the added value of assimilating the special observations. Note that the verification dataset used for the summer case is the same dataset used for obs nudging in MFDDA5; it is used for verifying all three experiments. Figures 10c and 10d show clear advantages of assimilating special surface wind, especially for the two finer grids. Upper-air statistics for this case were not available at the time of publication and will be included in the future.

## 6. CONCLUSIONS

This study evaluates the WRF model configurations for a winter case study and a summer case study over the west coast region centered over the Bay Area. Various configurations are systematically tested in order to find an optimal configuration that will produce reasonable model simulations both at the surface and in the upper-air. These best-performing model simulations will become the meteorological inputs for photochemical air quality models in order to optimize air quality simulations. The air quality simulations will lead to better air quality forecasts that will allow cities and states such as San Francisco and California to better prepare a response plan for high pollution events.

The goals of this study are achieved by comparing the use of different radiation physics, different land-surface models, and the combination of different FDDA strategies. The study shows that both the RRTM and the RRTMG radiation schemes perform similarly, and that there are no clear advantages to use the newly-introduced RRTMG scheme for the winter case. Therefore, the RRTM scheme is adopted for the atmospheric radiation physics as part of the best model configuration.

The study shows that the Pleim-Xiu (PX) land-surface model (LSM) gives the best results over the 5-layer thermal diffusion scheme, the Noah LSM, and the RUC LSM for the winter case, and is selected (along with the RRTM radiation scheme) to be part of the best model configuration. No particular LSM outperforms the others for the summer case. Because a LSM is needed for the air chemistry models, the PX LSM is also chosen for the summer case model simulations.

The FDDA simulations made for this study show that for both winter and summer cases a multiscale framework produces the best model simulations for both the surface and the upper-air. This multiscale framework involves using both 3D analysis nudging and surface analysis nudging in combination with observational nudging. There is added value when using the special surface observations from the BAAQMD surface meteorological network.

Additional studies can be performed to possibly improve the model simulations further. Correlation statistics can be computed to determine how well the errors between two observation sites are correlated with each other. This can help to determine an optimal radius of influence (RIN) for the data assimilation process. Future study should also include using independent datasets to verify the WRF solutions.

*Acknowledgements*. This research was funded by the Bay Area Air Quality Management District, under contract No. 2009-078. We also thank Brian Gaudet of Penn State for his help with the objective evaluation and statistical verification software, and we acknowledge Brian Reen of Penn State for his help with the adjustments made to the default WRF PBL model to fix noise issues and reduce model errors.

## 7. REFERENCES

Bao, J.-W., S. A. Michelson, P. O. G. Persson, I. V. Djalalova, J. M. Wilczak, 2008: Observed and WRF-simulated low-level winds in a high-ozone episode during the Central California Ozone Study. *J. Appl. Meteor. And Clim.*, **47**, 2373-2394.

Beaver, S., S. Tanrikulu, C. Tran, S. T. Soong, Y. Jia, R. Rogers, A. Deng, and D. R. Stauffer, 2011: Fine particulate matter modeling in Central California, Part II: Application of the Community Multiscale Air Quality model, 13th Conference on Atmospheric Chemistry, Seattle, WA, Jan. 23-27, 8 pp.

Benjamin, S., and N. L. Seaman, 2985: A simple scheme for objective analysis in curved flow. *Mon. Wea. Rev*. **113**, 1184-1198.

Chen, F., and J. Dudhia, 2001: Coupling an advanced land-surface/ hydrology model with the Penn State/ NCAR MM5 modeling system. Part I: Model description and implementation. *Mon. Wea. Rev.*, **129**, 569–585.

Deng, A., D.R. Stauffer, B.J. Gaudet, J. Dudhia, J. Hacker, C. Bruyere, W. Wu, F. Vandenberghe, Y. Liu and A. Bourgeois, 2009: Update on WRF-ARW end-to-end multi-scale FDDA system, *10th Annual WRF Users' Workshop*, Boulder, CO, June 23, 14 pp.

Deng, A., N. L. Seaman, G. K. Hunter and D. R. Stauffer, 2004: Evaluation of interregional transport using the MM5-SCIPUFF system. *J. Appl. Meteor.*, **43**, 1864-1886.

Dudhia, J., 1989: Numerical study of convection observed during the winter monsoon experiment using a mesoscale two-dimensional model, *J. Atmos. Sci*., **46**, 3077–3107.

Grell, G. A., J. Dudhia, and D. R. Stauffer, 1994: A description of the fifth generation Penn State/NCAR Mesoscale Model (MM5). NCAR Tech. Note NCAR/TN-3981STR, 138 pp.

Iacono, M., J. Delamere, E. Mlawer, M. Shephard, S. Clough, and W. Collins, 2008: Radiative forcing by long-lived greenhouse gases: Calculations with the AER radiative transfer models*, J. Geophys. Res*., **113**, D13103, doi:10.1029/2008JD009944.

Janjic, Z. I., 1996: The surface layer in the NCEP Eta Model, Eleventh Conference on Numerical Weather Prediction, Norfolk, VA, 19–23 August; Amer. Meteor. Soc., Boston, MA, 354–355.

Janjic, Z. I., 2002: Nonsingular Implementation of the Mellor–Yamada Level 2.5 Scheme in the NCEP Meso model, NCEP Office Note, No. 437, 61 pp.107.

Kain, J. S., and J. M. Fritsch, 1990: A one-dimensional entraining/ detraining plume model and its application in convective parameterization, *J. Atmos. Sci.*, **47**, 2784–2802.

Kain, J. S., 2004: The Kain-Fritsch convective parameterization: An update. *J. Appl. Meteor*., **43**, 170–181.

Mlawer, E. J., S. J. Taubman, P. D. Brown, M. J. Iacono, and S. A. Clough, 1997: Radiative transfer for inhomogeneous atmosphere: RRTM, a validated correlated-k model for the longwave*. J. Geophys. Res*., **102 (D14),** 16663–16682.

Otte, T. L., 2008a: The Impact of nudging in the meteorological model for retrospective air quality simulations. Part I: Evaluation against national observation networks. *J. Appl. Meteor. Climatol*., **47**, 1853-1867.

Otte, T. L., 2008b: The Impact of nudging in the meteorological model for retrospective air quality simulations. Part II: Evaluating collocated meteorological and air quality observations. *J. Appl. Meteor. Climatol*., **47**, 1868-1887.

Pleim, J. and R. Gilliam, 2009: An indirect data assimilation scheme for deep soil temperature in the Pleim–Xiu land surface model. *J. Appl.Meteor. Climatol*., **48**, 1362–1376.

Pleim, J. E. and A. Xiu, 1995: Development and testing of a surface flux and planetary boundary layer model for application in mesoscale models. *J. Appl. Meteor.*, 34, 16–32.

Skamarock, W.C., J.B. Klemp, J. Dudhia, D.O. Gill, D.M. Barker, M.G. Duda, X.-Y. Huang, W. Wang and J.G. Powers, 2008: A Description of the Advanced Research WRF Version 3. NCAR Tech. Note 475+STR, 113 pp.

Smirnova, T. G., J. M. Brown, and S. G. Benjamin, 1997: Performance of different soil model configurations in simulating ground surface temperature and surface fluxes. *Mon. Wea. Rev.*, **125**, 1870–1884.

Smirnova, T. G., J. M. Brown, S. G. Benjamin, and D. Kim, 2000: Parameterization of coldseason processes in the MAPS land-surface scheme. *J. Geophys. Res.*, **105 (D3),** 4077–4086.

Stauffer, D.R. and N.L. Seaman, 1994: Multiscale Four-Dimensional Data Assimilation. *J. Appl. Meteor.*, **33**, 416-434.

Tanrikulu, S., D.R. Stauffer, N.L. Seaman and A.J. Ranzieri, 2000: A Field-Program Design for Air-Quality Studies. Part II: Evaluation in the San Joaquin Valley. *J. App. Meteor*., **39**, 317-334.

Xiu, A. and J. E. Pleim, 2001: Development of a land surface model part I: Application in a mesoscale meteorology model. *J. Appl. Meteor.*, **40**, 192–209.

Table 1 – FDDA configuration for the six FDDA model simulations for the winter case

| Exp. Name | 36 km | | 12 km | | 4 km | |
|---|---|---|---|---|---|---|
| | Analysis Nudging | OBS Nudging | Analysis Nudging | OBS Nudging | Analysis Nudging | OBS Nudging |
| NOFDDA | NO | NO | NO | NO | NO | NO |
| GFDDA | YES | NO | Yes | NO | NO | NO |
| OFDDA | NO | YES | NO | YES | NO | YES |
| MFDDA | YES (3D) | YES | YES (3D) | YES | NO | YES |
| MFDDA2 | YES (3D+Sfc) | YES | YES (3D+Sfc) | YES | NO | YES |
| MFDDA3 | YES (3D+Sfc-soil) | YES | YES (3D+Sfc-soil) | YES | NO | YES |

Table 2 – FDDA parameters used for the winter case. Note that these parameters are also used for the summer case except that there is no observational nudging on the 36-km domain

| | Analysis Nudging | | | OBS Nudging | | |
|---|---|---|---|---|---|---|
| | 36km | 12km | 4km | 36km | 12km | 4km |
| G (1/sec) | 0.0003 | 0.0001 | N/A | 0.0004 | 0.0004 | 0.0004 |
| 3-D wind field | Nudging all layers | Nudging all layers | N/A | Nudging all layers | Nudging all layers | Nudging all layers |
| 3-D mass field | Nudging above PBL | Nudging above PBL | N/A | Nudging above PBL | Nudging above PBL | Nudging above PBL |
| Sfc wind field | Used within PBL | Used within PBL | N/A | Used within PBL | Used within PBL | Used within PBL |
| Sfc mass field | Not used | Not used | N/A | Not used | Not used | Not used |
| RINXY (km) | N/A | N/A | N/A | 150 | 100 | 100 |
| TWINDO (hr) | N/A | N/A | N/A | 2 | 2 | 2 |
| dt (sec) | N/A | N/A | N/A | 180 | 60 | 20 |

Table 3 – FDDA configuration for three FDDA model simulations for the summer case. *MFDDA5 assimilates both WMO and BAAQMD special surface data and MFDDA4 only assimilates WMO data.

| Exp. Name | 36 km | | 12 km | | 4 km | |
|---|---|---|---|---|---|---|
| | Analysis Nudging | OBS Nudging | Analysis Nudging | OBS Nudging | Analysis Nudging | OBS Nudging |
| NOFDDA | NO | NO | NO | NO | NO | NO |
| MFDDA4 | YES (3D+Sfc) | NO | YES (3D+Sfc) | YES | NO | YES |
| MFDDA5* | YES (3D+Sfc) | NO | YES (3D+Sfc) | YES | NO | YES |

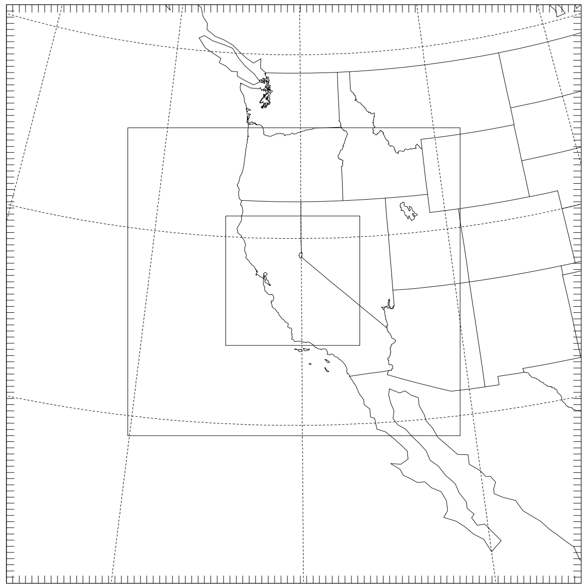

Figure 1 – Nested domains for the model simulations showing the 4-km (innermost), 12-km (middle) and 36-km (outermost) domains.

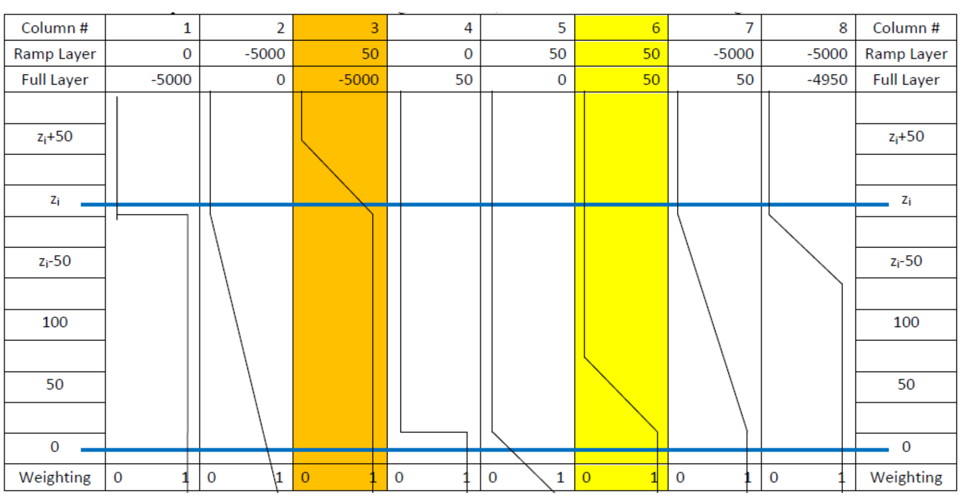


Figure 2 – Illustration of possible vertical weighting functions for surface observations. For each of the eight examples, the horizontal axis is the weight (from zero to one) and the vertical axis is height from 0 (the ground) to zi+50 (50 m above the top of the PBL). The settings used to produce the vertical weighting function are indicated in the second two rows. The blue horizontal lines indicate the surface and the PBL top. Column 6 is the default for the stable PBL regimes (regime 1 and 2), and column 3 is the default for the unstable PBL regime (regime 4).

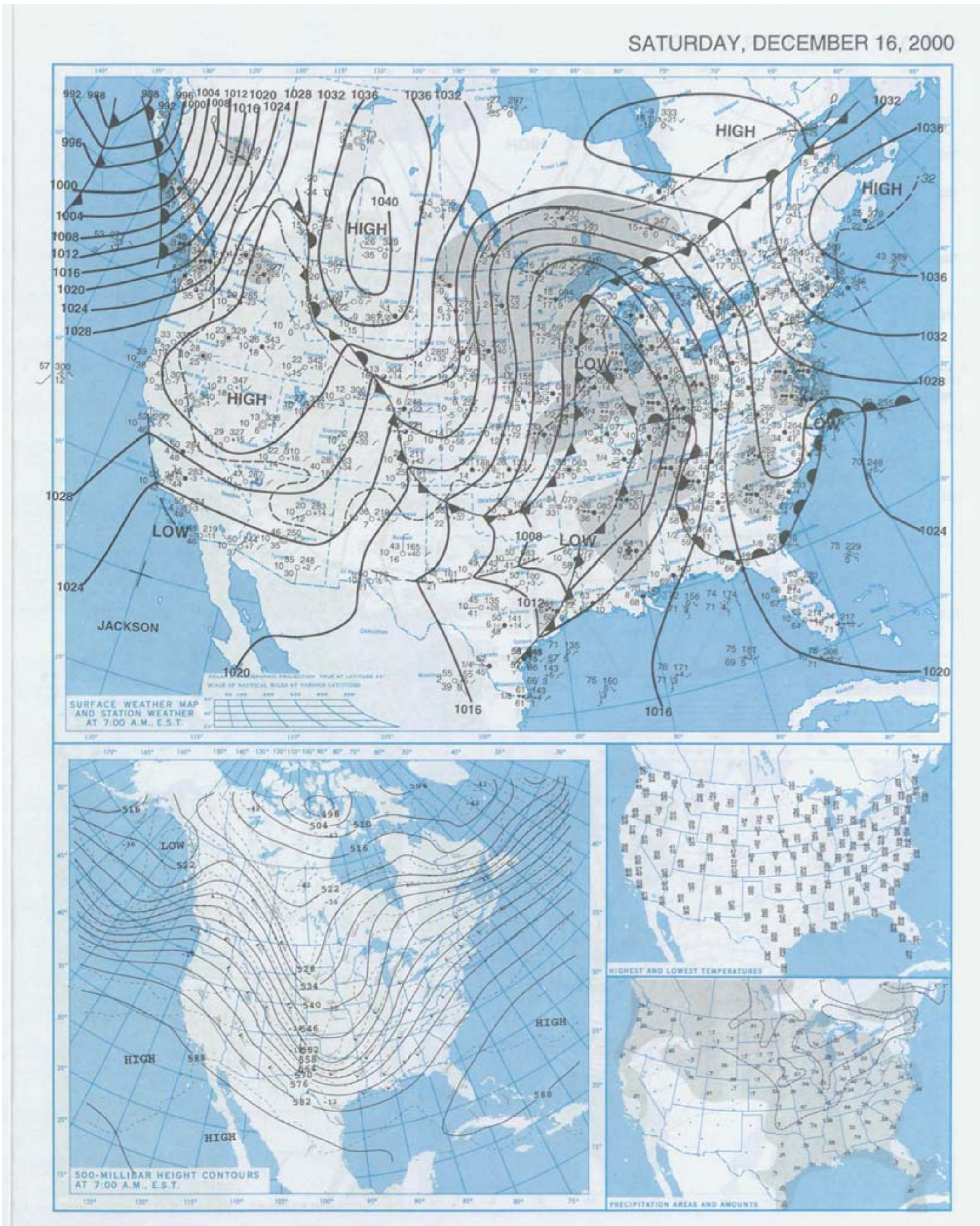


Figure 3: Surface (top) and 500 hPa (bottom left) observations for 12 UTC on December 16, 2000. (Source: *Daily Weather Maps* from the NOAA Central Library Data Imaging Project)

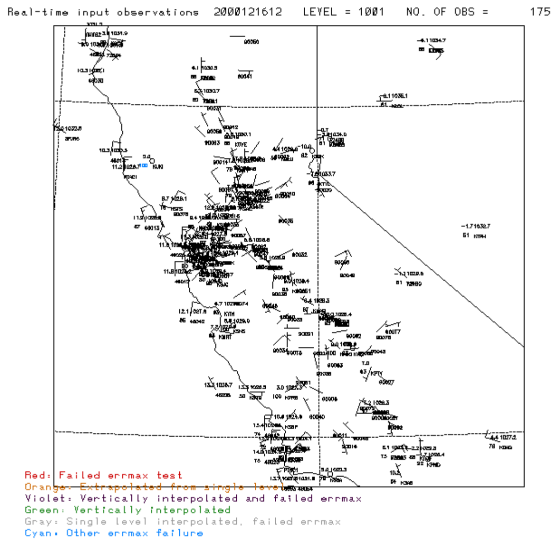


(a)

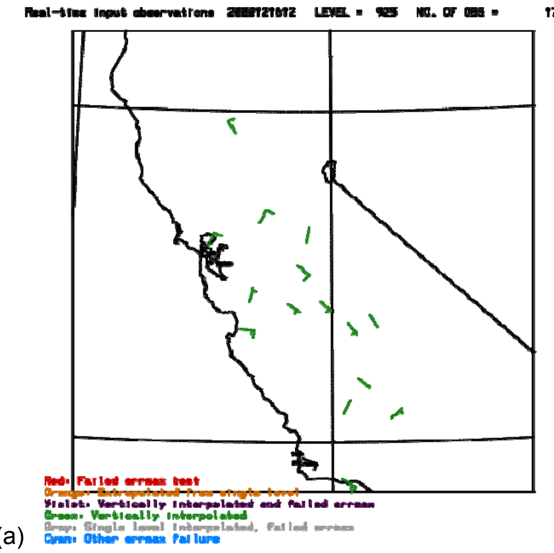


(b)

Figure 4 – Observational data used for data assimilation for the winter case. (a) WMO data and BAAQMD data for the surface. (b) WMO data and BAAQMD data for the upper-air.

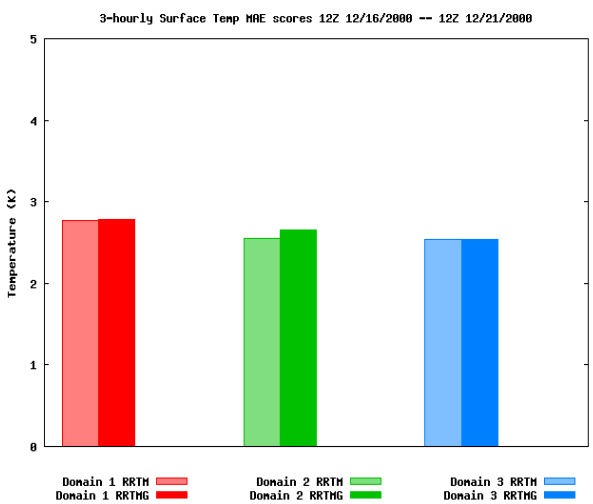


Figure 5 – MAE surface temperature (K) comparison between RRTM and RRTMG radiation schemes for the winter case.

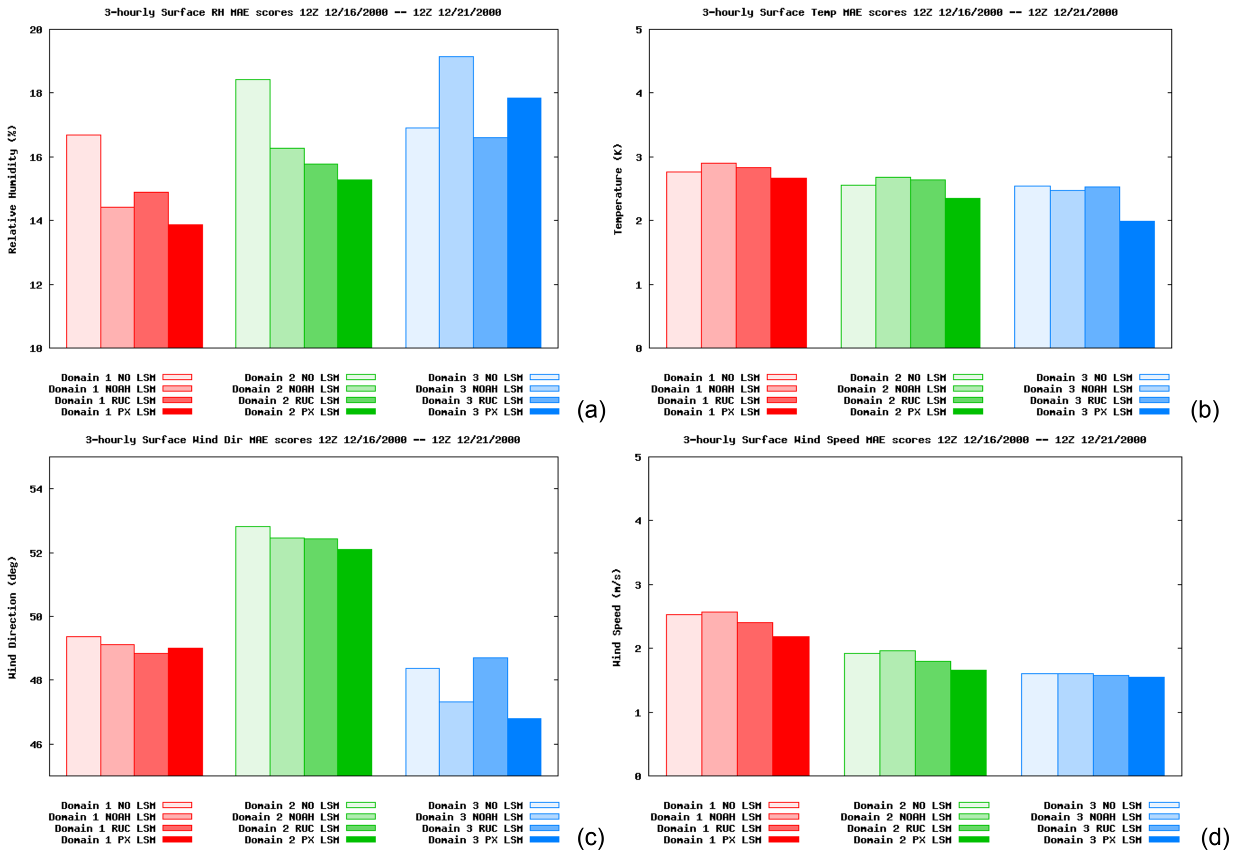


Figure 6 – Surface MAE comparison of the thermal diffusion LSM, Noah LSM, RUC LSM, and Pleim-Xiu LSM for the winter case. (a) Relative Humidity (percent), (b) Temperature (K), (c) Wind Direction (degrees), (d) Wind Speed (m/s)

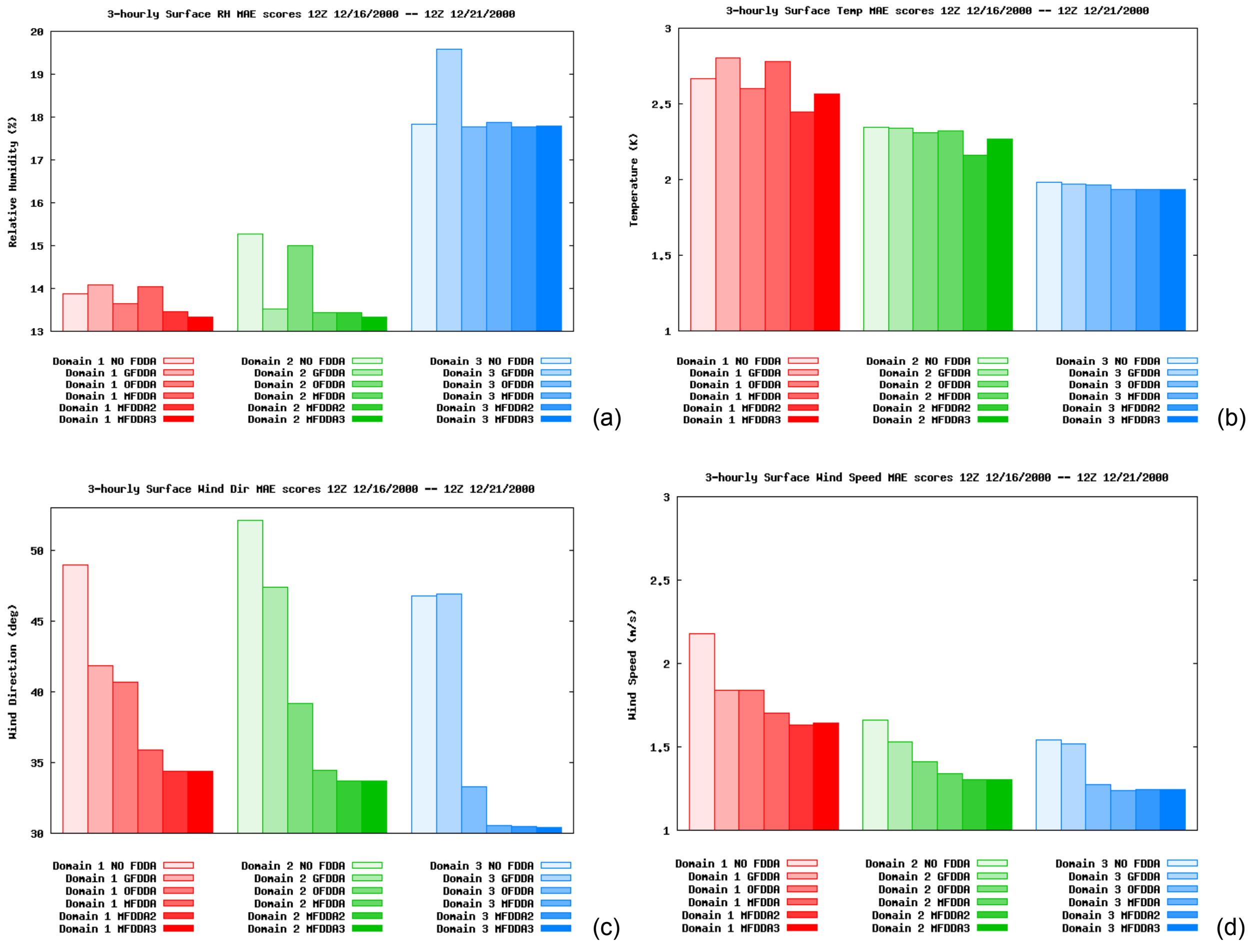


Figure 7 – Surface MAE comparison of the six FDDA model simulations for the winter case. (a) Relative Humidity (percent), (b) Temperature (K), (c) Wind Direction (degrees), (d) Wind Speed (m/s)

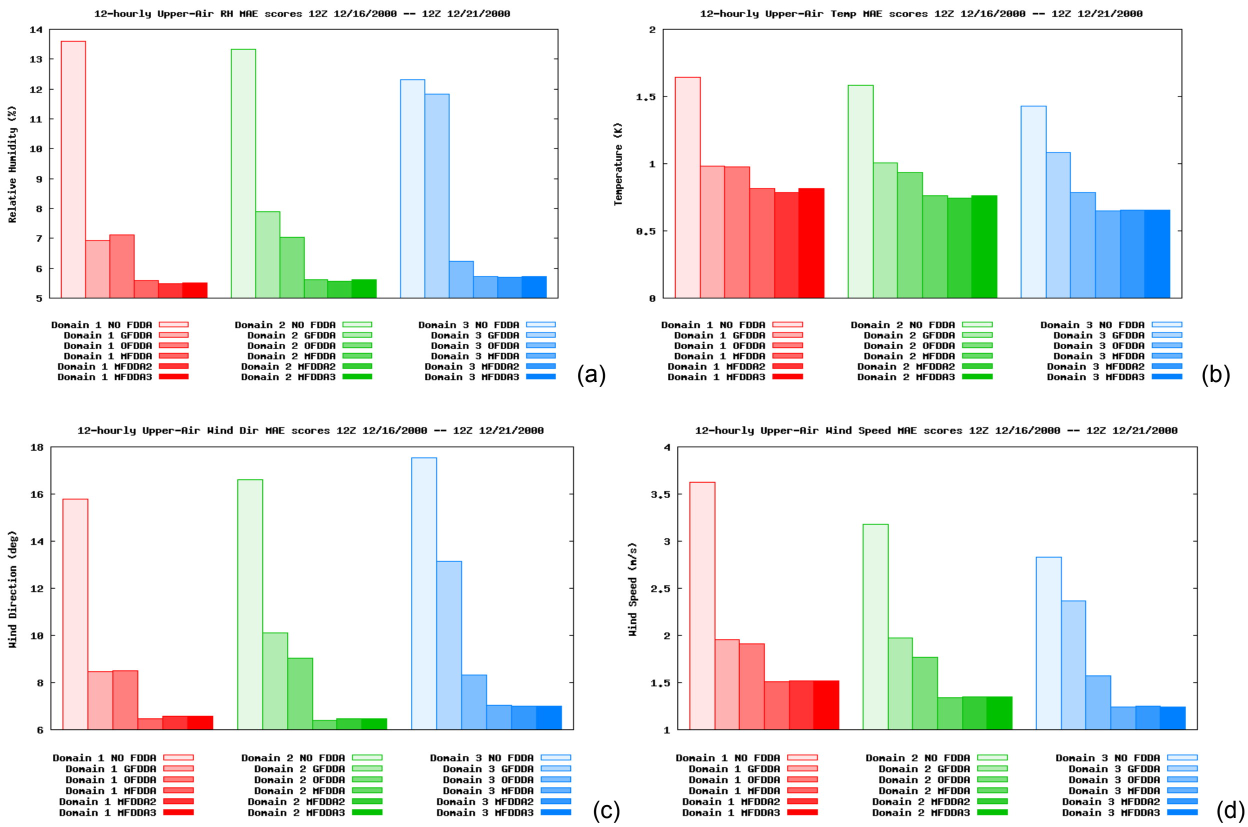


Figure 8 – Similar to Fig. 7 except for the upper-air statistics.

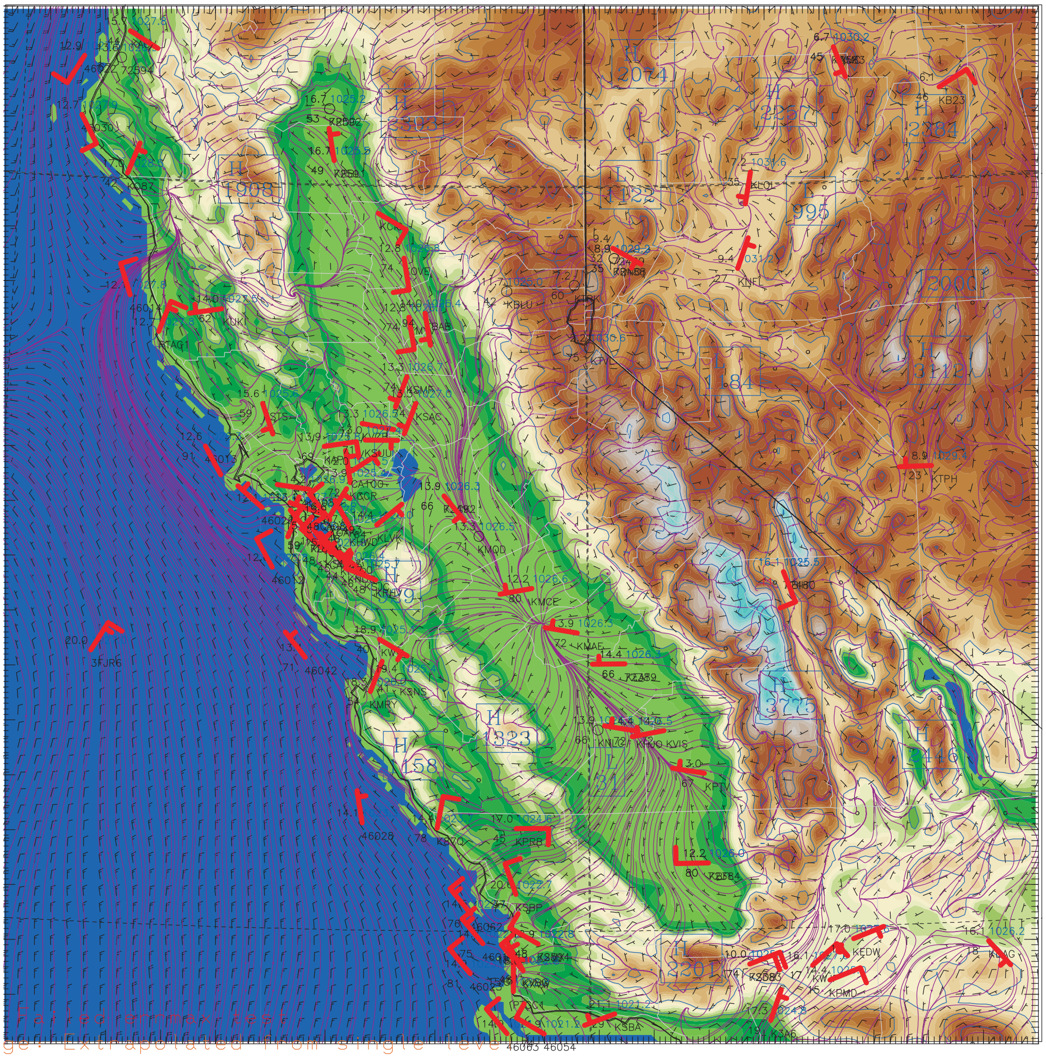

(a)

Figure 9 – Plots of the model simulated surface winds on the 4-km domain for the winter case at 00 UTC on December 17, 2000 (4 p.m. PST). (a) a no-FDDA simulation and (b) an FDDA simulation (Expt. MFDDA2).

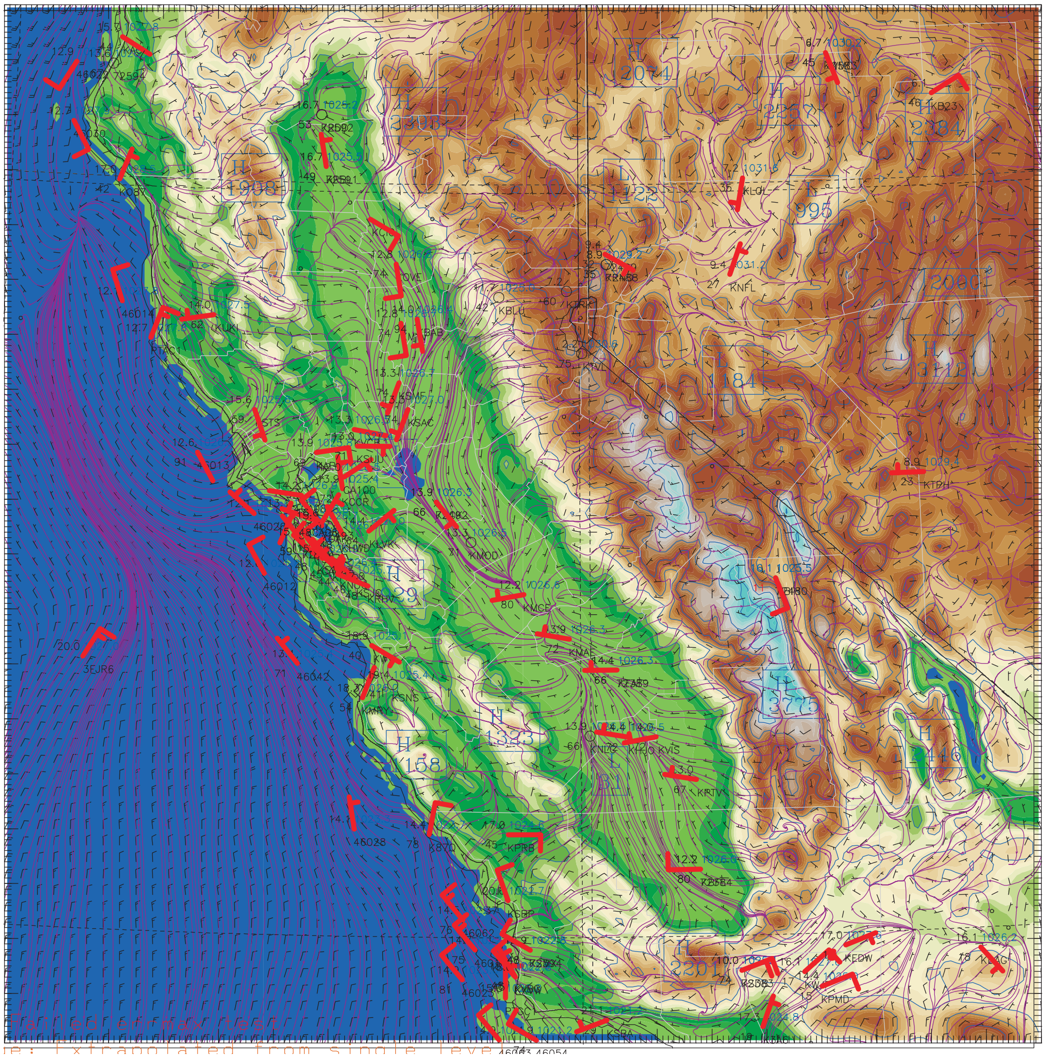

(b)

Figure 9 – Continued.

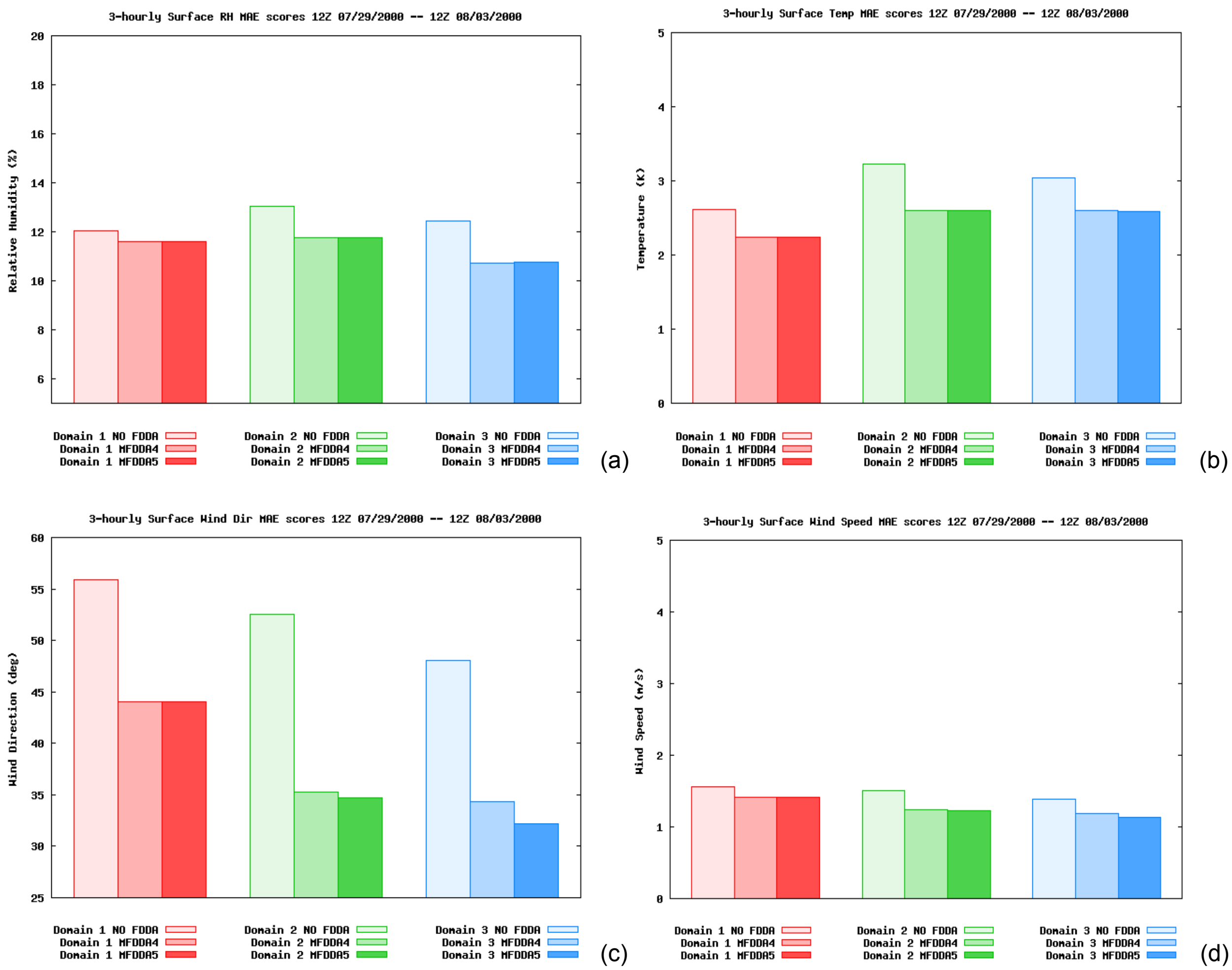


Figure 10 – Surface MAE comparison of the three FDDA model simulations for the summer case. (a) Relative Humidity (percent), (b) Temperature (K), (c) Wind Direction (degrees), (d) Wind Speed (m/s)